Journal of Computational and Applied Mathematics 259 (2014) 651–659

Contents lists available at ScienceDirect

Journal of Computational and Applied Mathematics

journal homepage: www.elsevier.com/locate/cam

Parallel implicit DNS of temporally-evolving turbulent shear layer instability

Ilyas Yilmaz [a,*,1], Firat Oguz Edis [b], Hasan Saygin [c], Lars Davidson [d]

[a] Energy Institute, Istanbul Technical University, Maslak, 34469, Istanbul, Turkey

[b] Department of Astronautical Engineering, Faculty of Aeronautics and Astronautics, Istanbul Technical University, Maslak, 34469, Istanbul, Turkey

[c] Department of Mechanical Engineering, Faculty of Engineering and Architecture, Istanbul Aydin University, Florya, 34295, Istanbul, Turkey

[d] Division of Fluid Dynamics, Department of Applied Mechanics, Chalmers University of Technology, Göteborg, SE-412 96, Sweden

HIGHLIGHTS

- An all-Mach/all-speed method was applied to the transition to turbulence and mixing.
- An algorithmic improvement to its convergence properties was made.
- An in-house, fully implicit, fully parallel DNS solver was developed.
- The physics of the transition to turbulence and mixing was successfully captured.
- A proper amount of dissipation is required at high Mach numbers for stability.

ARTICLE INFO

Article history:
Received 24 January 2013
Received in revised form 19 March 2013

Keywords:
DNS
TSL
Parallel
Implicit
All-speed
Compressibility

ABSTRACT

In this study, a temporally-evolving incompressible and compressible Turbulent Shear Layer (TSL) instability problem is solved using an all-speed (all-Mach), implicit, non-dissipative and kinetic energy conserving algorithm. An in-house, fully parallel, finite-volume Direct Numerical Simulation (DNS) solver was developed using PETSc. Convergence characteristics at low-Mach numbers were also improved using a relaxation procedure. We aim here to assess the performance and behavior of the present algorithm for complex flows which contain multi-scale physics and gradually evolve into turbulence. The results show that the algorithm is able to produce correct physical mechanisms and capture the evolution of the turbulent fluctuations for both incompressible and compressible cases. It is observed that the non-dissipative and kinetic energy conserving properties make the algorithm powerful and applicable to challenging problems. For higher Mach numbers, a shock-capturing or a dissipative mechanism is required for robustness.

1. Introduction

We present a three-dimensional Direct Numerical Simulation (DNS) study of mixing in temporally-evolving Turbulent Shear Layer (TSL) instability. For this purpose, an in-house, fully parallel, finite-volume DNS solver, *i*DNS, was developed,

* Corresponding author. Tel.: +90 212 444 1 428/1766.
E-mail addresses: yilmazily@itu.edu.tr, ilyasyilmaz@aydin.edu.tr (I. Yilmaz), edis@itu.edu.tr (F.O. Edis), hasansaygin@aydin.edu.tr (H. Saygin), lada@chalmers.se (L. Davidson).
1 Present address: Department of Mechanical Engineering, Faculty of Engineering and Architecture, Istanbul Aydin University, Florya, 34295, Istanbul, Turkey.

0377-0427/$ – see front matter © 2013 Elsevier B.V. All rights reserved.
http://dx.doi.org/10.1016/j.cam.2013.04.002

based on a fully implicit, non-dissipative, and discrete kinetic energy conserving algorithm recently proposed by Hou and Mahesh [1]. The PETSc library was utilized for an efficient parallelism [2].

Our aim here is twofold: first, to demonstrate the algorithm's ability to evolve perturbations into turbulent mixing for the base flow with the convective Mach number $M_c = 0.3$, and, second, to analyze the effects of compressibility on the growth rate of the instability by increasing the convective Mach number.

The following sections include a brief review of the algorithm with a further improvement in convergence, the solver details, the definition and the numerical setup of the problem. The results obtained are analyzed and compared to those from previous experimental and numerical studies.

2. The numerical method

The algorithm solves the set of time-dependent, three-dimensional compressible Navier–Stokes equations. These are non-dimensionalized by using the reference values. Unlike in many other methods, pressure is non-dimensionalized, as $p = \frac{p^d - p_{ref}}{\rho_{\mathrm{ref}} u_{ref}^2}$, which is known as *incompressible scaling* or *low-Mach number scaling* [3,4]. The resulting non-dimensional forms of the equations satisfy the incompressibility condition, and allow to study low-Mach number flows with the same algorithm without encountering the acoustic stiffness problem, when the Mach number goes to zero. The algorithm is second-order in both space and time on orthogonal grids. It is stable and robust at high-Reynolds numbers [1]. It is a *pressure-correction* type of algorithm which uses an *iterative predictor–corrector* approach to update the flow variables. The variables are stored at the cell centers. A fully implicit, finite-volume discretization is used. The discretization is centered in both space and time to ensure the non-dissipativeness. Thermodynamic quantities such as density, pressure, and temperature are also staggered in time by half a time step relative to the velocities [5]. The values of the variables at cell faces are obtained by *symmetric interpolation*, which is the simple averaging of two adjacent cell-center values. This also ensures the conservation of kinetic energy discretely at the low-Mach number limit [6]. The *face-normal velocity*, V_n, is treated as a separate flow variable like the velocity and is updated in time [7,8]. V_n is stored at the center of the cell faces directly to mimic the staggered grids, to prevent odd–even decoupling in pressure in space. In order to give a fully implicit treatment of pressure, the algorithm works with a weighted sum of previous, current, and predicted values of the pressure, instead of the pressure itself directly [5]. An additional correction to pressure is also adopted in the algorithm to enhance the convergence properties by preventing possible successive oscillating pressure corrections in time [9]. This procedure provides a time- and space-dependent relaxation factor for the pressure at the end of each time-step for low-Mach number flows.

3. Solver details

In order to perform this study, an in-house, fully parallel DNS solver, *i*DNS, was developed based on the algorithm mentioned above and the PETSc parallel library. *i*DNS is a single-block, structured, fully implicit, finite-volume solver working on uniform Cartesian grids. Fig. 1 shows the flowchart of *i*DNS and the iterative solution procedure as well. It consists of three parts: *pre-processing, core* and *post-processing*. In *pre-processing*, the PETSc framework is initialized. Grid related quantities and initial conditions for the simulations are generated. *Core* performs all steps for the solution of the discretized equations. *Post-processing* calculates necessary quantities for analyzing and comparison, and also stores them into files. *i*DNS was written in a modular fashion using Fortran syntax. The linear systems arising from the discretization are first *pre-conditioned* by incomplete-LU with zero-filling (ILU(0)), and are then solved using GMRES. During the parallel performance tests, very good speed-up and efficiency results were obtained. Tests also showed that the solver is scalable, since it maintains the efficiency when increasing the problem size and the number of cores.

4. The problem definition and setup

Turbulent shear layers are of interest for many physical and engineering flows such as jets, wakes and mixing in combustion. They are induced by strong gradients in the shear stress. Although they have a relatively simple configuration, complex physical phenomena are included in these flows. They are mostly dominated by large-scale, quasi-2D, organized structures. However, they can rapidly undergo transition to turbulence in 3D. The first theoretical analyses were presented in the 50's and 60's [10]. Experimental investigations began in the 70's [11,12], and this was followed by early DNS simulations in the 80's and 90's [13,14] with the help of the advances in computer technology. Recently, well-resolved numerical simulations were performed [15,16]. There has remained an ongoing interest in turbulent shear layers and need for better understanding of their physical mechanisms, due to the requirements of flight (such as in wake control) and combustion technologies (such as in supersonic mixing), for developing more efficient systems [17]. They can be studied both spatially and temporally. In spatially-evolving mixing layers, mixing layer thickness of two emerging streams of fluids develops in the streamwise direction. Such development requires a large extent of the domain. This is computationally much more expensive to track than the temporally-evolving mixing layers where the thickness of the layer increases as a function of time rather than as a function of the streamwise coordinate.

The flow is initialized with a hyperbolic tangent function for the mean streamwise velocity, $\bar{u} = \frac{\Delta u}{2} \tanh\left(-\frac{y}{2\delta_\theta(0)}\right)$, where $\delta_\theta(0)$ is *the initial momentum thickness*. This defines two parallel streams moving in opposite directions with the same

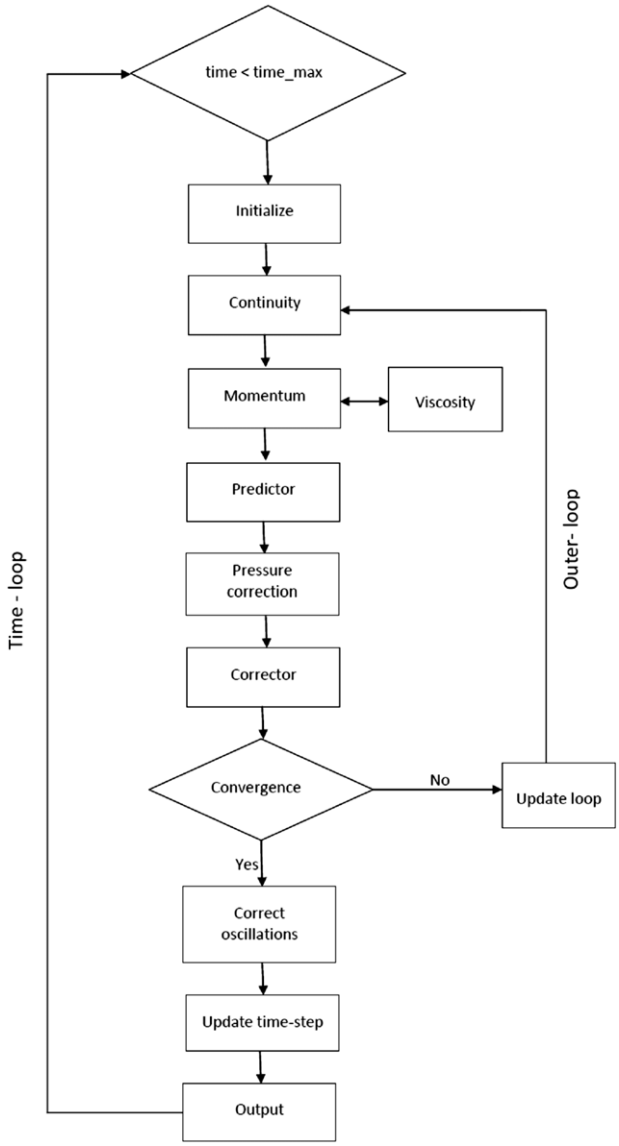

Fig. 1. Flowchart of *i*DNS.

velocity, $\frac{\Delta u}{2}$, where Δu is the velocity difference between the lower and the upper streams. It is also taken as the reference velocity. The normalwise (y) and the spanwise (z) mean velocities are set to zero. The initial densities are equal for the two streams and are set to unity. The initial pressure is uniform as well. It is set to give the speed of sound as unity and is chosen as the reference pressure. The Reynolds number based on the initial momentum thickness, Re_θ, the velocity difference, and the average dynamic viscosity is 160 and the Reynolds number based on the initial vorticity thickness ($\delta_\omega(0)$), Re_ω, is 680. The ratio of the specific heats, γ, is 1.4 and the Prandtl number, Pr, is 0.72. The density ratio between streams is equal to 1. Different convective Mach numbers are studied. The idea of the convective Mach number was first introduced in order to identify the effects of compressibility on the shear-layer growth rate. For equal densities and specific heats, it can be written as $M_c = \frac{\Delta u}{c_1+c_2}$, where c_1 and c_2 denote the speeds of sound for each of the streams.

The initial momentum thickness is taken as the reference length scale. The reference scale is $\tau = \frac{\delta_\omega(0)}{\Delta u}$.

The boundary conditions are periodic in the streamwise (x) and spanwise (z) directions. Inviscid slip-wall boundary conditions are used at bottom and top boundaries in the normalwise (y) direction. The face-normal velocities require special treatment and must be set to zero on inviscid slip-walls.

The non-dimensional time-steps are set to 6×10^{-3} for the quasi-incompressible case where M_c is 0.3, 1×10^{-2} for the mildly-compressible cases where $M_c = 0.5$, 0.7, and 5×10^{-3} for the highly compressible case where $M_c = 0.9$. The flow was followed up to the very late non-linear stage, and then the simulation was stopped.

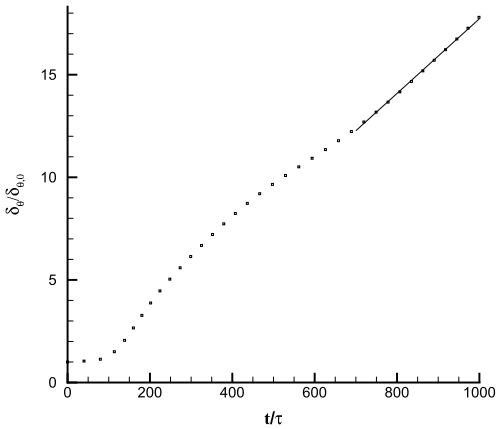

Fig. 2. Time evolution of momentum thickness for $M_c = 0.3$.

The same problem domain as was considered by Pantano and Sarkar [16] is used for our computations. The domain is very large, especially in the streamwise direction, in order to allow the flow to evolve into a self-similar state. This resolution is also sufficient for representing the large-scale structures in the flow, as shown by the same authors using a calculation of the integral length scales (which are sufficiently small compared to the domain size in homogeneous directions) and two-point correlations (which are decorrelated over half the domain size in homogeneous directions) in the self-similar state. The domain size is given in terms of the initial momentum thickness as $L_x \times L_y \times L_z = 345\delta_\theta(0) \times 172\delta_\theta(0) \times 86\delta_\theta(0)$ with corresponding resolution $N_x \times N_y \times N_z = 512 \times 256 \times 128$ for the cases considered. The initial momentum thickness is set to 0.093. A uniform orthogonal grid is used.

In addition to these mean values, turbulent three-dimensional velocity fluctuations are superimposed on the initial mean velocity components. The fluctuations are generated on the basis of a technique described by Davidson [18] using the isotropic turbulence energy spectrum, $E(\kappa) = u'^2_{rms}(\frac{\kappa}{\kappa_0})^4 \exp(-2(\frac{\kappa}{\kappa_0})^4)$, where κ_0 is the *peak wave-number*. κ_0 is adjusted so as to have 48 peak wavelengths in the streamwise direction for the simulations. u'_{rms} denotes the *rms* of the velocity fluctuations and is given as $u'_{rms} = (ti \cdot \Delta u)$ where *ti* is the turbulent intensity which is set to 0.1. The initial turbulent velocity fluctuating field obtained is limited to the shear layer by multiplying with a shape function in the form $\exp(-(\frac{y}{2\delta_\theta(0)})^2)$. The runs were performed on distributed memory architectures with Intel Xeon dual-core and quad-core processors. 256 cores with 2 GB of RAM per core were used for the simulations. The total wall-clock time was 350–500 h, depending on M_c. Since the implicit algorithm allows larger time steps as given above, this computational time is quite acceptable and possibly much shorter than for an explicit method.

5. Results and discussion

5.1. The quasi-incompressible case

The quasi-incompressible case ($M_c = 0.3$) is chosen as the base case. This case is also used for the code verification, and the comparison as well. In order to analyze the results, the momentum thickness, δ_θ, is first introduced as

$$\delta_\theta = \frac{1}{\rho_0 \Delta u^2} \int_{-\infty}^{+\infty} \overline{\rho} \left(\frac{1}{2}\Delta u - \tilde{u}_1\right)\left(\frac{1}{2}\Delta u + \tilde{u}_1\right) dy \tag{1}$$

where $\tilde{u}_1$ denotes the Favre averaged streamwise velocity component and $\overline{\rho}$ is the Reynolds averaged density.

As an integral quantity, the momentum thickness is less sensitive to statistical noise than the vorticity thickness, $\delta\omega = \frac{\Delta u}{(\frac{\partial \tilde{u}}{\partial y})_{\max}}$, and evolves smoothly in time [14]. The growth rate can be found as the slope of a linear curve fit, $\dot{\delta_\theta} = \frac{1}{\Delta u}\frac{d\delta_\theta}{dt}$.

The time evolution of the momentum thickness is given in Fig. 2. After an initial settling period, which mainly depends on the initial fluctuations, an approximate linear growth is observed, in consistency with the previous results. The growth rate is 0.0182 which is calculated by taking the slope of the curve in the region where the flow is self-similar. Pantano and Sarkar [16] obtained 0.0184 for the quasi-incompressible case from a DNS database. They also obtained 0.016 in their DNS study at $M_c = 0.3$. Our value is in good agreement with Pantano and Sarkar [16].

The Reynolds stress transport equation is introduced as in [16] to calculate the Reynolds stress tensor and the turbulent kinetic energy budget

$$\frac{\partial(\bar{\rho}R_{ij})}{\partial t} + \frac{\partial(\bar{\rho}\tilde{u}_k R_{ij})}{\partial x_k} = \bar{\rho}(P_{ij} - \epsilon_{ij}) - \frac{\partial T_{ijk}}{\partial x_k} + \Pi_{ij} \tag{2}$$

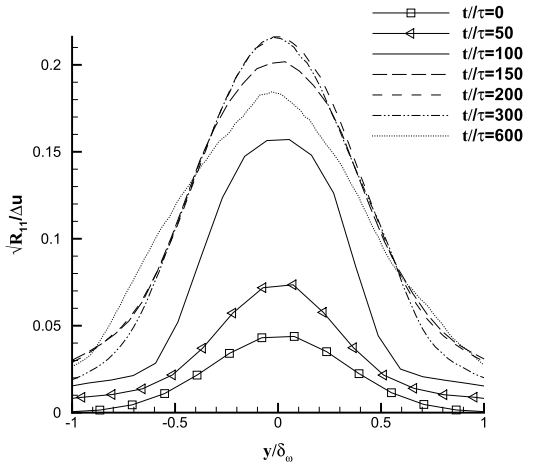

Fig. 3. Time evolution of $\sqrt{R}_{11}$.

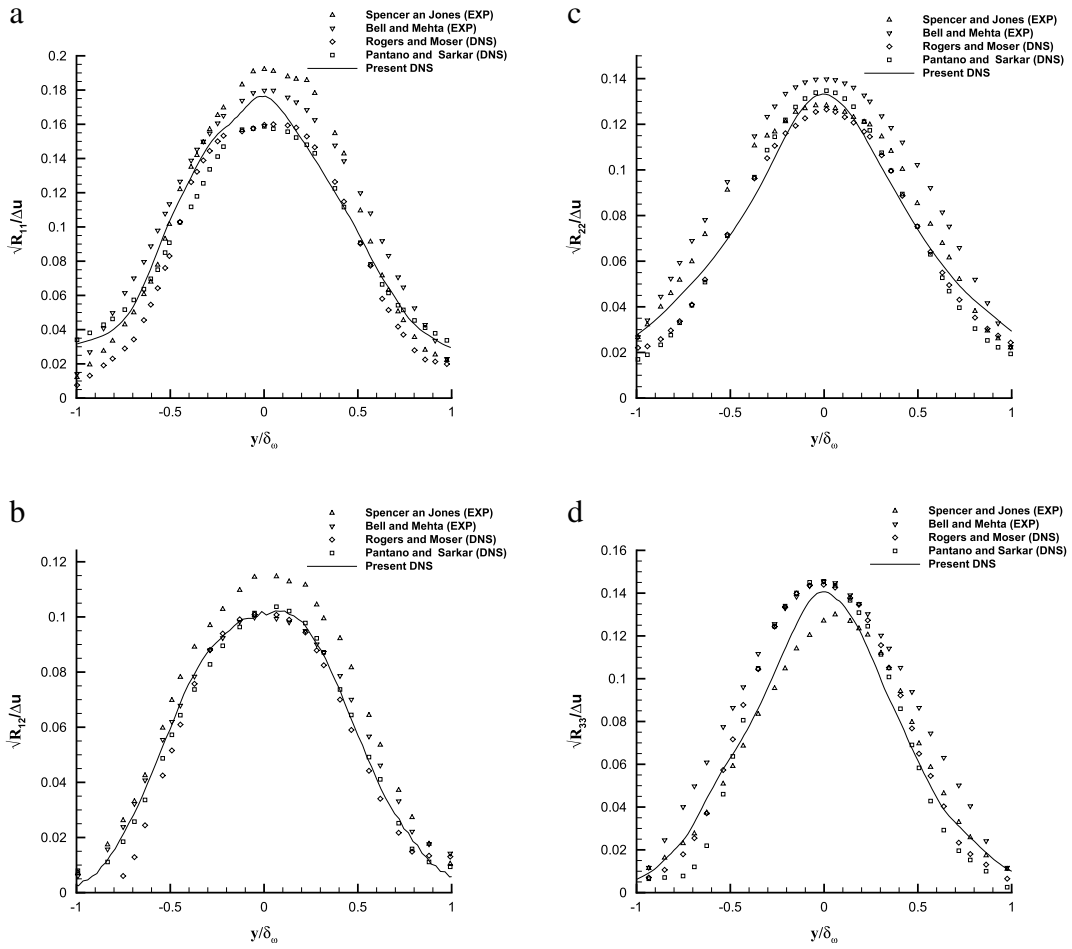

Fig. 4. Comparison of the Reynolds stresses for $M_c = 0.3$.

where R_{ij}, P_{ij}, ϵ_{ij}, T_{ijk}, Π_{ij} are turbulent stress, production, dissipation, transport and pressure–strain terms, respectively. Explicit forms and calculations of these terms can be found in [16].

Fig. 3 shows the time evolution of the *rms* of the velocity fluctuations in the streamwise direction. In consistency with the previous studies, it starts from an initial value, reaches a peak and then decreases to its specific value. The comparisons of the Reynolds stresses are given in Fig. 4—compared with those from experiments and other DNS studies. A procedure of

Table 1
Comparison of the peaks of the Reynolds stresses for $M_c = 0.3$.

	$\sqrt{R_{11}}/\Delta u$	$\sqrt{R_{22}}/\Delta u$	$\sqrt{R_{33}}/\Delta u$	$\sqrt{R_{12}}/\Delta u$
Bell and Mehta [19] (EXP, $M_c = 0$)	0.180	0.140	0.146	0.100
Pantano and Sarkar [16] (DNS)	0.155	0.134	0.143	0.103
Hadjadj et al. [20] (LES)	0.170	0.134	0.143	0.106
Foysi and Sarkar [21] (LES)	0.174	0.129	0.143	0.106
Present DNS	0.176	0.133	0.141	0.102

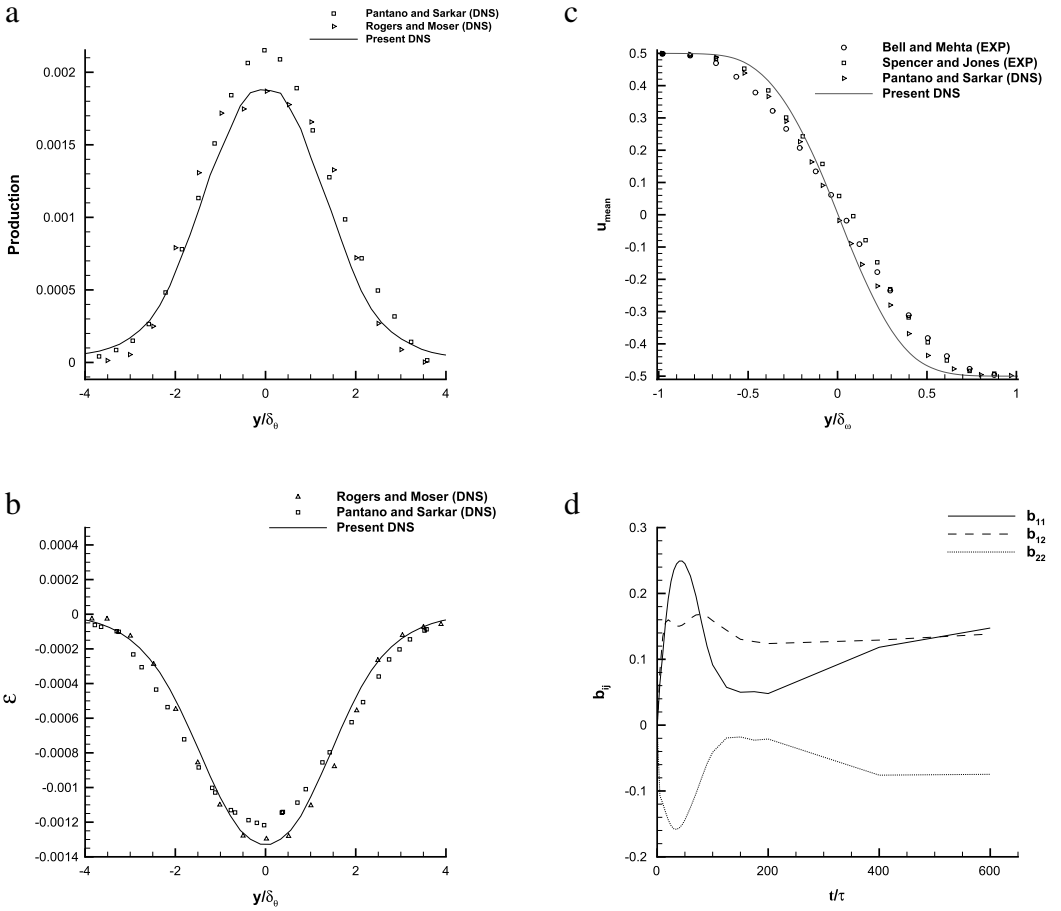

Fig. 5. Comparison of the production (a), dissipation (b), mean streamwise velocity (c), and time evolution of anisotropy terms (d) for $M_c = 0.3$.

averaging over the time period between 200 and 600 was applied. As can be seen, the agreement is good. The streamwise component of the Reynolds stress is larger than the other components. Table 1 compares the peak turbulent intensities of the Reynolds stresses to those from some prior numerical studies. Our DNS gives similar values to the others. Turbulent production and dissipation are presented in Fig. 5(a) and (b). Our values are in good agreement with those from the other DNS studies [16,14].

Fig. 5(c) shows the mean velocity in the streamwise direction and it is compared to those from previous experimental and numerical studies. u_{mean} is again obtained via an averaging between $t/\tau = 200$ and $t/\tau = 600$. The agreement with other data is good.

The anisotropy of the Reynolds stresses shows the character and the dependence of the velocity fluctuations on the direction in turbulent flows. Once Reynolds stress terms are calculated, it can be obtained via $b_{ij} = \frac{R_{ij}}{2K} - \frac{1}{3}\delta_{ij}$, where K is the turbulent kinetic energy and δ_{ij} is the Kronecker delta. It is calculated by integrating over the shear layer [16], which is approximated by summation.

Time evolutions of the anisotropy of the Reynolds stress terms are also given in Fig. 5(d). Table 2 compares their peak values to those from the Large-Eddy Simulation (LES) of Foysi and Sarkar [21] and DNS of Pantano and Sarkar [16]. In the self-similar region (i.e., after a sufficiently long time), the values of the diagonal components of b_{ij} reach a constant value.

Table 2
Comparison of the peaks of the Reynolds stress anisotropies for $M_c = 0.3$.

	b_{11}	b_{22}	b_{12}
Foysi and Sarkar [21] (LES)	0.35	−0.20	0.21
Pantano and Sarkar [16] (DNS)	0.26	−0.16	0.19
Present DNS	0.25	−0.16	0.17

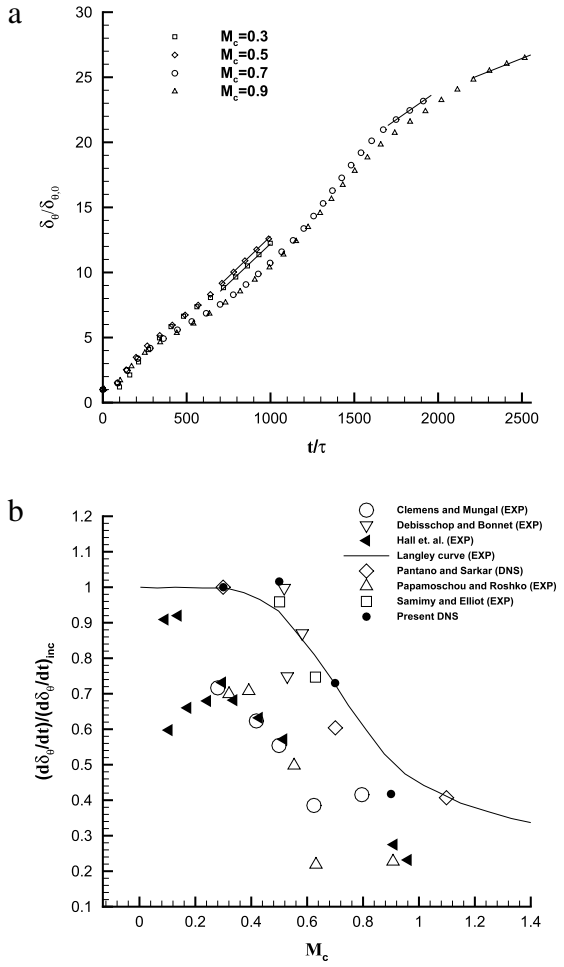

Fig. 6. Comparison of the momentum thicknesses (a) and the growth rates (b) for different values of M_c.

The present peak values are very close to those of Pantano and Sarkar [16]. The anisotropy in the streamwise direction is stronger than those in the other directions.

5.2. The compressible cases

In the previous section it was demonstrated for the base quasi-incompressible case that the algorithm and the solver produce the correct physical mechanisms behind the TSL instability. In the following cases, the behavior of the algorithm in the presence of compressibility effects is investigated. For this purpose, variations of M_c between 0.3 and 0.9 are studied. The results are presented and are compared with those from previous experimental and numerical studies. Compressibility effects are also analyzed.

Fig. 6(a) compares the time evolutions of the momentum thicknesses for different convective Mach numbers. A linear fit for each curve is plotted in the self-similar region for calculation and comparison of the growth rates. It is observed that the time required to obtain to a self-similar state increases with increasing M_c. The growth rate values are normalized by the base incompressible growth rate value and are plotted against M_c in Fig. 6(b). The filled circles represent our results. As is

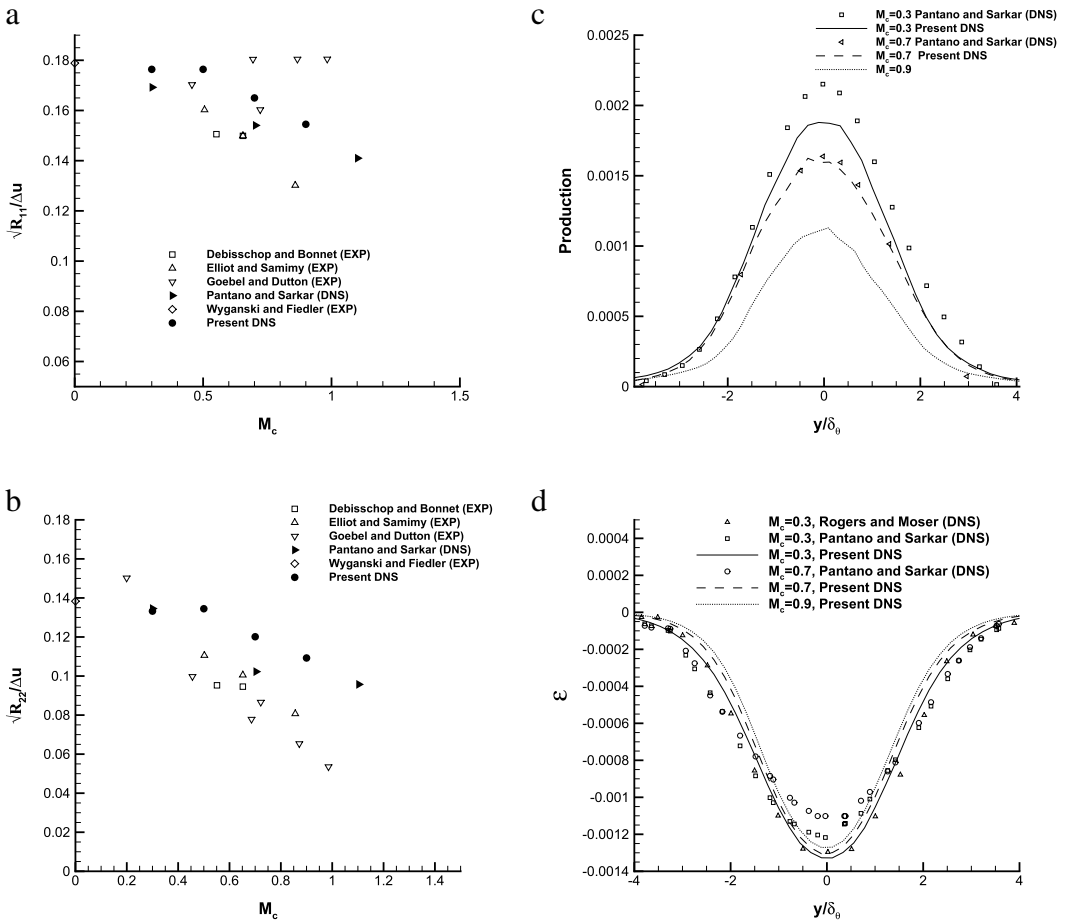

Fig. 7. The effect of compressibility on the various terms of the Reynolds stress transport equation.

clearly seen, the compressibility reduces the growth rate of the instabilities, agreeing well with many previous results and the widely accepted Langley experimental curve represented by solid line [16,22–26].

Fig. 7 shows that the compressibility effects reduce the Reynolds stress terms, production and dissipation, which is consistent with the previous studies [16,14,21,27]. The reduction in production is the source of the decrease in the growth rate, as confirmed by the other DNS studies [16,14,21]. The turbulent dissipation is less affected by the compressibility than the other terms, as previously noted in [16,21]. A slight increase is observed in the peak values of the Reynolds stress anisotropies at early times. The diagonal components are more affected than the off-diagonal ones. The overall effect of increasing M_c on the values of b_{ij} is not large, which is consistent with previous numerical studies [16,21].

6. Conclusions

An in-house, fully parallel DNS solver, *i*DNS, was developed, based on a fully implicit, non-dissipative, discrete kinetic energy conserving, all-speed flow algorithm, and was successfully applied to temporally-evolving Turbulent Shear Layer (TSL) problem.

TSL simulation results prove that the algorithm is capable of capturing the evolution of the perturbations into a non-linear hydrodynamic state which can be regarded as the onset of the turbulence. By doing this study, we performed further assessment of the algorithm and examined its behavior and applicability to these kinds of flows, including complex spatial and temporal multi-scale physics. All the results compare well to the previous experimental and numerical results. It seems that non-dissipativeness and discrete kinetic energy conserving properties work well. The improved convergence characteristic obtained via a time- and space-relaxed procedure for the pressure saves computational resources and prevents the loss of accuracy at low-Mach numbers. A dissipative mechanism is necessary for studying higher Mach numbers. However, single, unified approaches are very attractive for solving such complex problems.

Acknowledgments

Computing resources used in this work were provided by the National Center for High Performance Computing of Turkey (UYBHM) under grant number 1001212011 and TUBITAK–ULAKBIM, High Performance and Grid Computing Center (TRUBA

Resources). Since an earlier part of the work was carried out at Chalmers University of Technology during the first author's research visit, IY thanks to Istanbul Technical University and The Scientific and Technological Research Council of Turkey (TUBITAK) for supporting his stay. The financial support of SNIC (Swedish National Infrastructure for Computing) during this period for computer time at C3SE (Chalmers Center for Computational Science and Engineering) under the Project SNIC001-10-22 is also gratefully acknowledged.

References

[1] Y. Hou, K. Mahesh, A robust, colocated, implicit algorithm for direct numerical simulation of compressible, turbulent flows, Journal of Computational Physics 205 (2005) 205–221.
[2] S. Balay, W.D. Gropp, L.C. McInnes, B.F. Smith, Efficient management of parallelism in object oriented numerical software libraries, in: E. Arge, A.M. Bruaset, H.P. Langtangen (Eds.), Modern Software Tools in Scientific Computing, Birkhäuser Press, 1997, pp. 163–202.
[3] F. White, Viscous Fluid Flow, McGraw-Hill, 1991.
[4] P. Wesseling, Principles of Computational Fluid Dynamics, Springer-Verlag, 2001.
[5] C. Wall, C.D. Pierce, P. Moin, A semi-implicit method for resolution of acoustic waves in low mach number flows, Journal of Computational Physics 181 (2002) 545–563.
[6] S. Benhamadouche, K. Mahesh, G. Constantinescu, Colocated finite-volume schemes for large-eddy simulation on unstructured meshes, in: Proceedings of the 2002 Summer Program, Center for Turbulence Research, Stanford University and NASA Ames, 2002.
[7] D. Kim, H. Choi, A second-order time-accurate finite volume method for unsteady incompressible flow on hybrid unstructured grids, Journal of Computational Physics 162 (2000) 411–428.
[8] Y. Zang, R.L. Street, J.R. Koseff, A non-staggered grid, fractional step method for time-dependent incompressible Navier–Stokes equations in curvilinear coordinates, Journal of Computational Physics 114 (1994) 18–33.
[9] G. Walton, AIRNET—a computer program for building airflow network modeling, Technical Report NISTIR 89-4072, National Institute of Standards and Technology, 1989.
[10] S. Chandrasekhar, Hydrodynamic and Hydromagnetic Stability, in: International Series of Monographs on Physics, Clarendon Press, 1961.
[11] I. Wygnanski, H.E. Fiedler, The two-dimensional mixing region, Journal of Fluid Mechanics 41 (1970) 327–361.
[12] B.W. Spencer, B.G. Jones, Statistical investigation of pressure and velocity fields in the turbulent two-stream mixing layer, in: AIAA Paper 71-613.
[13] J. Riley, R. Metcalfe, Direct numerical simulation of a perturbed turbulent mixing layer, in: AIAA Paper 80-0274.
[14] M.M. Rogers, R.D. Moser, Direct simulation of a self-similar turbulent mixing layer, Physics of Fluids 6 (1994) 903–923.
[15] A.W. Vreman, Direct and large eddy simulation of the compressible turbulent mixing layer, Ph.D. Thesis, University of Twente, 1995. http://search.proquest.com/docview/304209114?accountid=11638.
[16] C. Pantano, S. Sarkar, A study of compressibility effects in the high-speed turbulent shear layer using direct simulation, Journal of Fluid Mechanics 451 (2002) 329–371.
[17] J. Steelant, Long-term advanced propulsion concepts and technologies II, LAPCAT-II. http://cordis.europa.eu/search/index.cfm?fuseaction=proj.document&PJ_RCN=10335111 (accessed: 06.03.13).
[18] L. Davidson, Using isotropic synthetic fluctuations as inlet boundary conditions for unsteady simulations, Advances and Applications in Fluid Mechanics 1 (2007) 1–35.
[19] J.H. Bell, R.D. Mehta, Development of a two-stream mixing layer from tripped and untripped boundary layers, AIAA Journal 28 (1990) 2034–2042.
[20] A. Hadjadj, H.C. Yee, B. Sjögreen, LES of temporally evolving mixing layers by an eighth-order filter scheme, International Journal for Numerical Methods in Fluids 70 (2012) 1405–1427.
[21] H. Foysi, S. Sarkar, The compressible mixing layer: an LES study, Theoretical and Computational Fluid Dynamics 24 (2010) 565–588.
[22] J.R. Debisschop, J.P. Bonnet, Mean and fluctuating velocity measurements in supersonic mixing layers, in: Engineering Turbulence Modeling and Experiments 2: Proceedings of the Second International Symposium on Engineering Turbulence Modeling and Measurement, Elsevier, 1993.
[23] M. Samimy, G.S. Elliot, Effects of compressibility on the characteristics of free shear layers, AIAA Journal (1990) 439–445.
[24] D. Papamoschou, A. Roshko, The compressible turbulent shear layer: an experimental study, Journal of Fluid Mechanics 197 (1988) 453–477.
[25] N.T. Clemens, M.G. Mungal, Large-scale structure and entrainment in the supersonic mixing layer, Journal of Fluid Mechanics 284 (1995) 171–216.
[26] J.L. Hall, P.E. Dimotakis, H. Rosemann, Experiments in non-reacting compressible shear layers, AIAA Journal (1990) 2247–2254.
[27] R.D. Moser, M.M. Rogers, The three-dimensional evolution of a plane mixing layer: pairing and transition to turbulence, Journal of Fluid Mechanics 247 (1993) 275–320.